

See discussions, stats, and author profiles for this publication at: <https://www.researchgate.net/publication/8114056>

# Virtual Screening of Human 5-Aminoimidazole-4-carboxamide Ribonucleotide Transformylase against the NCI Diversity Set by Use of AutoDock to Identify Novel Nonfolate Inhibitors

ARTICLE *in* JOURNAL OF MEDICINAL CHEMISTRY · JANUARY 2005

Impact Factor: 5.45 · DOI: 10.1021/jm049504o · Source: PubMed

---

CITATIONS

51

---

READS

93

5 AUTHORS, INCLUDING:



Chenglong Li

The Ohio State University

140 PUBLICATIONS 2,749 CITATIONS

SEE PROFILE



Dennis W Wolan

The Scripps Research Institute

27 PUBLICATIONS 796 CITATIONS

SEE PROFILE

# Virtual Screening of Human 5-Aminoimidazole-4-carboxamide Ribonucleotide Transformylase against the NCI Diversity Set by Use of AutoDock to Identify Novel Nonfolate Inhibitors<sup>†</sup>

Chenglong Li,<sup>‡</sup> Lan Xu,<sup>‡</sup> Dennis W. Wolan,<sup>‡</sup> Ian A. Wilson,<sup>\*,‡,§</sup> and Arthur J. Olson<sup>\*,‡</sup>

Department of Molecular Biology and Skaggs Institute for Chemical Biology, The Scripps Research Institute, 10550 North Torrey Pines Road, La Jolla, California 92037

Received June 22, 2004

AICAR transformylase (5-aminoimidazole-4-carboxamide ribonucleotide transformylase) is a folate-dependent activity of the bifunctional protein ATIC (AICAR transformylase and IMP cyclohydrolase) and is responsible for catalyzing the penultimate step of the *de novo* purine biosynthetic pathway. As such, AICAR transformylase has been proposed as a potential target for antineoplastic drug design. Virtual screening of the human AICAR transformylase active site by use of AutoDock against the NCI diversity set, a library of compounds with nonredundant pharmacophore profiles, has revealed 44 potential inhibitor candidates. *In vitro* inhibition assay of 16 soluble compounds from this list revealed that eight compounds with novel scaffolds, relative to the general folate template, had micromolar inhibition. Subsequent extension of docking trials on compounds with similar scaffolds from the entire NCI-3D database has unveiled 11 additional inhibitors that were confirmed by the *in vitro* inhibition assay. In particular, one compound, NSC30171, had nanomolar inhibition ( $K_i = 154$  nM,  $IC_{50} = 600$  nM) against AICAR transformylase. These 19 inhibitors serve as novel templates/scaffolds for development of more potent and specific non-folate-based AICAR transformylase inhibitors.

## Introduction

Folate-dependent enzymes are required for cell division and tissue growth in mammals.<sup>1</sup> Likewise, antifolates have been shown to downregulate tissue growth and cellular proliferation, as exemplified by their use in treating various neoplastic diseases. In addition, antifolates can be used in the treatment of microbial infections, inflammatory disorders, and autoimmune diseases. The main antifolate targets include four folate-dependent enzymes: dihydrofolate reductase (DHFR),<sup>2,3</sup> thymidylate synthase (TS),<sup>4,5</sup> glycylamide ribonucleotide transformylase (GAR Tfase),<sup>6–10</sup> and 5-aminoimidazole-4-carboxamide ribonucleotide transformylase (AICAR Tfase).<sup>11</sup>

We have primarily focused on the purine nucleotide *de novo* biosynthetic pathway because rapidly dividing cancer cells rely mainly on the *de novo* synthesis of nucleotides rather than the more economical salvage pathway due to the requirement of significant amount of purines to sustain rapid growth.<sup>12</sup> Two folate-dependent enzymes in this pathway, GAR Tfase and AICAR Tfase, are responsible for transferring a formyl group from the folate cofactor to substrate. GAR Tfase converts glycylamide ribonucleotide (GAR) to formylglycylamide ribonucleotide (FGAR) in step 3, while AICAR Tfase adds the formyl group onto the 5-amino position of 5-aminoimidazole-4-carboxamide ribonucleotide (AICAR) to form the stable intermediate 5-formylaminoimidazole-4-carboxamide ribonucleotide (FAICAR) in step 9.<sup>11</sup> FAICAR is ultimately cyclized to the final product of the pathway, inosine monophosphate (IMP) (Figure 1), by

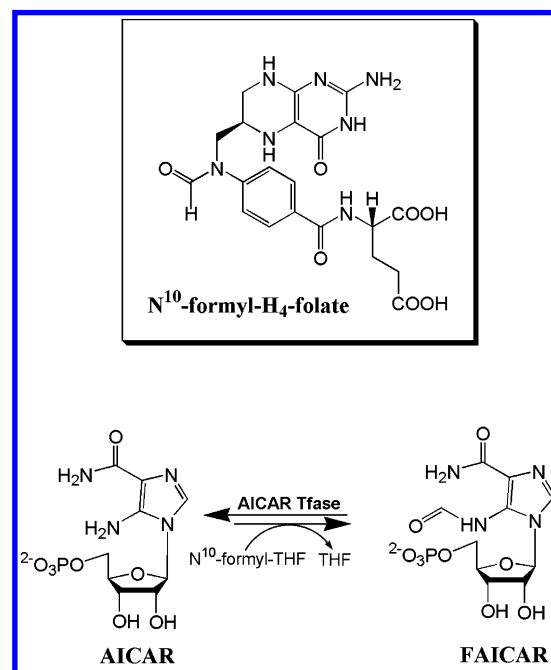


Figure 1. Conversion of AICAR to FAICAR by AICAR Tfase.

the IMP cyclohydrolase activity of ATIC (the bifunctional enzyme comprising AICAR transformylase and IMP cyclohydrolase). Inhibition of enzymes within this pathway can induce accumulation of intermediates prior to that particular step and depletion of downstream intermediates, a “metabolic crossover point”.<sup>13</sup> The resulting imbalance of deoxynucleotides (dNTPs) may lead to genetic miscoding,<sup>14</sup> and/or complete depletion of one of the dNTPs that would arrest DNA synthesis. Thus, a cell exposed to such a nucleotide antagonist eventually die due to accumulated mutations or DNA strand breaks, usually via apoptosis.<sup>15–17</sup>

<sup>†</sup> This is publication 16701-MB from The Scripps Research Institute.

<sup>\*</sup> Correspondence may be addressed to either author: (I.A.W.) e-mail wilson@scripps.edu; phone (858) 784-9706; fax (858) 784-2980, (A.J.O.) e-mail olson@scripps.edu; phone (858) 784-9702; fax (858) 784-2860.

<sup>‡</sup> Department of Molecular Biology.

<sup>§</sup> Skaggs Institute for Chemical Biology.

GAR Tfase was initially validated as an anticancer target in the mid-1980s with the discovery of a potent and selective inhibitor, 5,10-dideaza-5,6,7,8-tetrahydrofolate (DDATHF).<sup>18</sup> The C-6 *R* isomer of DDATHF, Lometrexol, specifically inhibits GAR transformylase ( $K_i$  60 nM) and can inhibit AICAR transformylase to a lesser extent ( $K_i > 10 \mu\text{M}$ ).<sup>18–20</sup> Clinical trials demonstrated antitumor activity against a wide range of solid tumors, which are the most difficult forms of cancer to combat.<sup>19</sup> However, strong side effects caused by folate deficiency<sup>21</sup> resulted in its withdrawal from further clinic trials. Additionally, the actions of certain nonsteroidal anti-inflammatory drugs (NSAIDs), as well as the anti-inflammatory effects of the antifolate methotrexate (MTX), have been attributed in part to inhibition of AICAR Tfase activity.<sup>22–24</sup> NSAIDs and MTX cause intracellular accumulation of AICAR and dihydrofolate derivatives, which inhibits adenosine deaminase and adenosine kinase, enhancing adenosine release at the inflammatory site. Adenosine diminishes inflammation via occupancy of A2 receptors on inflammatory cells.<sup>22,25</sup> Moreover, recent studies show that AICAR accumulation can activate adenosine monophosphate-activated kinase (AMPK), a key regulator of cellular energy homeostasis. This leads to the inhibition of protein synthesis associated with hypertrophy in cardiac myocyte,<sup>26</sup> improved insulin sensitivity,<sup>27</sup> and anti-inflammatory effects by inhibiting lipopolysaccharide- (LPS-) induced expression of pro-inflammatory cytokines (tumor necrosis factor  $\alpha$ , interleukin- $1\beta$ , and interleukin-6) and inducible nitric oxide synthase in primary rat astrocytes, microglia, and peritoneal macrophages.<sup>28</sup>

Few clinically useful antifolates have been disclosed and even fewer of them have become marketable drugs despite the considerable discovery efforts over the past decade. The reasons may be 3-fold: (a) it is difficult to design and develop antifolates for one specific target only [development of drug binding to just one target is always desirable, despite the recent success of pemetrexed (Alimta), which broadly inhibits all folate-dependent enzymes<sup>29</sup>]; (b) the inhibitors cannot pass ADME/Tox tests, as in the case of Lometrexol; (c) most efforts have been focused to date on DHFR, TS, and GAR Tfase, not AICAR Tfase.<sup>19,30,31</sup> The folate scaffold has been used in the development of antineoplastic agents as these analogues can take advantage of the cellular reduced folate carrier (RFC1) and folate receptor<sup>32</sup> for transport into the cell. Subsequent polyglutamation of these folate analogues by FPGS (folypolyglutamate synthetase) potentiates drug retention and inhibition of folate-dependent enzymes by the increase of their negative charges and  $K_i$  values against TS, GAR Tfase, and AICAR Tfase. However, no conclusive studies have indicated that anti-folate polyglutamation is a crucial and desirable metabolic process that improves the therapeutic index.<sup>33</sup> For example, antifolates DDATHF and MTX are efficiently polyglutamated by FPGS and exhibit severe toxicity, as opposed to a nonpolyglutamatable DHFR inhibitor 4'-methylene-10-deazaaminopterin (MDAM) that exhibits superior antitumor activity and less toxicity.<sup>34</sup>

Thus, given the above considerations, we believe that pursuit of novel nonfolate AICAR Tfase inhibitors is a viable alternative. Crystal structures of both apo- and

holo-AICAR Tfase<sup>35–38</sup> show that the active-site conformation of the AICAR Tfase varies little upon ligand interaction, validating the efficacy of structure-based/computer-aided inhibitor design in this case. Here, we undertook virtual screening of the NCI diversity set against the human AICAR Tfase active site, to search for novel, nonfolate, nonpolyglutamatable classes of inhibitors. Indeed, we found several promising novel leads from the NCI diversity set<sup>39</sup> and from the larger NCI-3D database by using the AutoDock molecular docking simulation programs.<sup>40–42</sup>

## Materials and Methods

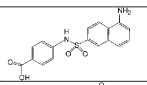
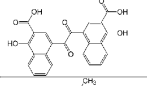
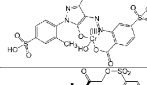
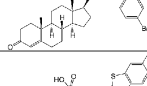
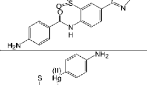
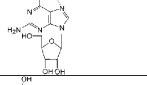
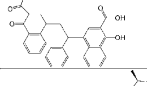
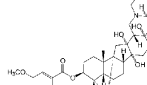
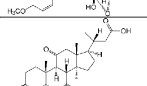
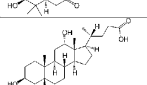
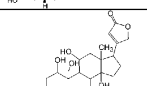
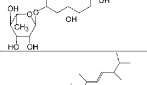
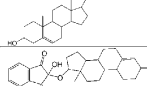
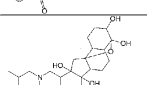
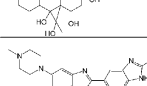
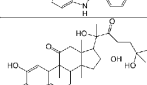
**Target Preparation.** Four AICAR Tfase crystal structures were available at the initiation of this study: apo avian ATIC (AICAR Tfase and IMP cyclohydrolase, PDB 1G8M),<sup>35</sup> avian ATIC in complex with AICAR substrate (PDB 1M9N),<sup>36</sup> avian ATIC with a multisubstrate adduct inhibitor (MAI) (PDB 1OZO),<sup>37</sup> and human ATIC in complex with the AICAR substrate and BW1540U88UD, a sulfonyl-containing antifolate (PDB 1P4R).<sup>38</sup> The human AICAR Tfase/BW1540 complex was selected as the docking template. Prior to docking studies, AICAR, BW1540, and crystallographic waters were removed. Polar hydrogens were added and all histidine residues were made neutral. The hydrogens on the histidine imidazole side chains were assigned as follows: HD1 on His 267, 385, 469, 584, and 592; HE2 on His 213, 290, 293, 453, 470, and 591. Kollman charges<sup>43</sup> were assigned to all atoms. Of the two identical active sites from the functional AICAR Tfase homodimer, the active site with lower average *B*-values were chosen for the docking site.  $60 \times 50 \times 66$  3D affinity grids centered on the active site with 0.375 Å spacing were calculated for each of the following atom types: C, A (aromatic C), N, O, S, H, F, Cl, Br, I, P, and e (electrostatic) by use of Autogrid3.<sup>42</sup>

**NCI Diversity Set.** The NCI diversity library is a reduced set of 1990 compounds selected from the original NCI-3D structural database for their unique scaffolds. The selection process is outlined in more detail at the NCI Developmental Therapeutic Program website.<sup>39</sup> Briefly, the diversity compounds were selected on the basis of their properties as unique three-point pharmacophores. All hydrogens were added and Gasteiger charges were assigned.<sup>44</sup> The rotatable bonds were assigned via AutoTors.<sup>42</sup>

**Screening Protocol.** AutoDock version 3.0.5<sup>42</sup> was used for the docking simulation. We selected the Lamarckian genetic algorithm (LGA) for ligand conformational searching because it has enhanced performance relative to simulated annealing or the simple genetic algorithm. The ligand's translation, rotation, and internal torsions are defined as its state variables, and each gene represents a state variable. LGA adds local minimization to the genetic algorithm, enabling modification of the gene population. For each compound, the docking parameters were as follows: trials of 100 dockings, population size of 150, random starting position and conformation, translation step ranges of 1.5 Å, rotation step ranges of 35°, elitism of 1, mutation rate of 0.02, crossover rate of 0.8, local search rate of 0.06, and 10 million energy evaluations. The jobs were distributed to the Scripps Atlas SGI Origin 2000 cluster, the NBCR Meteor, and the UCSD Keck/KeckII linux clusters. Final docked conformations were clustered by use of a tolerance of 1.5 Å root-mean-square deviation (RMSD). The top 44 compounds with the best simulated binding energies within the standard deviation of 2.1 kcal/mol were selected for the AICAR Tfase inhibition assay.

**Preparation of *N*<sup>10</sup>-Formyltetrahydrofolate and Enzymatic Inhibition Assay.** *N*<sup>10</sup>-Formyltetrahydrofolate (10-f-Thf) was prepared with a modified procedure by Rowe<sup>45</sup> and Black et al.,<sup>46</sup> and the human AICAR Tfase inhibition assay was performed as previously described.<sup>47,48</sup> IC<sub>50</sub> values were measured in a solution constituting of 25 nM ATIC, 50  $\mu\text{M}$  AICAR, and 8.5  $\mu\text{M}$  10-f-Thf. The detailed procedure is explained elsewhere.<sup>49</sup>

**Table 1.** AICAR Tfase Inhibitors from NCI Diversity Set Identified from Virtual Screening

Chemical structure	NSC number	MW	Rotatable bonds	% lowest energy Clustering	E <sub>binding</sub> (Kcal/mol)	IC <sub>50</sub> (μM)
	37173	342	5	88	-12.5	4.1 ± 0.3
	292213	430	7	68	-13.5	8.8 ± 0.1
	326203	607	7	4	-11.9	11.6 ± 0.1
	88915	550	5	40	-14.4	13.9 ± 1.4
	26699	440	6	76	-13.0	16.9 ± 1.8
	321237	591	8	47	-10.9	105.9 ± 6.2
	326211	508	7	54	-13.7	203.7 ± 4.4
	7524	674	13	62	-10.6	231.3 ± 17.6
	1614	447	4	51	-12.1	inactive
	8797	393	6	48	-13.3	inactive
	25485	585	12	36	-12.2	inactive
	62791	397	6	60	-12.8	inactive
	72254	435	3	64	-13.0	inactive
	99804	510	7	89	-11.5	inactive
	322921	534	4	82	-14.7	inactive
	521777	515	7	25	-12.8	inactive

**Similarity Compound Searching.** Once an inhibition was verified by the enzymatic inhibition assay, a compound search was similarly performed on the whole NCI-3D compound library constituting of 213 628 compounds. The compounds with larger than 70% similarity index were docked via the same docking protocol as described above. Again, the compounds with optimal binding according to the docking simulations were selected for *in vitro* kinetic inhibition verification. The URL for the similarity search is <http://chem.sis.nlm.nih.gov/nci3d/>, and the details of the NCI-3D database building and compound searching process have been described elsewhere.<sup>50</sup>

## Results

**Inhibitors from the NCI Diversity Set.** Forty-four compounds were selected for *in vitro* evaluation on the

basis of the computational simulation of free energy of binding to the AICAR Tfase. The simulated free energy differences among these compounds are within the 2.1 kcal/mol standard deviation of the AutoDock scoring function.<sup>42</sup> Prior to the enzymatic inhibition analysis, 10 NCI compounds were found to be water-insoluble, while 18 compounds precipitated in the assay buffer. Therefore, only 16 compounds could be experimentally testable for their inhibition potency against AICAR Tfase activity. Their chemical structures, NSC numbers, molecular weights, IC<sub>50</sub> values, and simulated binding free energies are listed in Table 1. Surprisingly, eight out of these 16 soluble compounds were shown to be AICAR Tfase inhibitors, resulting in a virtual screening



success rate of 50% with AutoDock. Five out of the eight inhibitors, NSC37173, NSC292213, NSC32-6203, NSC88915, and NSC26699, exhibited low micromolar  $IC_{50}$  values.

For the eight compounds that did not show kinetic inhibition of the AICAR Tfase activity, their simulated binding energies comprised primarily van der Waals contributions. Thus, simply "space-filling" the active site does not appear to predict reliable inhibition, at least in the case of AICAR Tfase. Furthermore, it appears that the active site/ligand interactions of the eight inhibitors are due to strong electrostatic, hydrogen-bonding, and aromatic interactions. In these cases, it then appears possible to design potent inhibitors with low molecular weight.

**NSC37173.** This compound had the lowest  $IC_{50}$  (4.1  $\mu$ M) and lowest molecular weight (342 Da) from the first-round diversity set screening. Two docking simulations were performed, one with the empty AICAR Tfase active site and one with the AICAR substrate occupying the substrate binding site and with the folate binding site empty (Figure 2A). Both show only one docking conformational cluster, indicating very high confidence of predictions. Its predicted binding modes to the AICAR Tfase are shown in Figure 2B. The two binding modes are very similar, except that the benzylcarboxyl tail flips out of the AICAR substrate binding site in the latter case. Crystal structure determinations are underway to confirm these predictions. Key electrostatic, aromatic, and hydrogen-bonding interactions explain the observed low  $IC_{50}$ : (a) The sulfonamide link strongly interacts with the "oxyanion hole" (Lys266, Arg451, and the backbone -NH amide of Arg451) in the center of the active site. This "oxyanion hole" most probably plays a crucial role in the stabilization of the transition state during the enzymatic formyl transfer reaction, similar to the "oxyanion hole" of  $\alpha/\beta$  hydrolases.<sup>51</sup> (b) The naphthalene ring interacts with the Phe544 benzyl ring and the carboxylate-connecting benzene ring interacts with the Phe316 side chain. Phe544 holds the naphthalene ring in the folate pterin binding pocket. The Phe591 benzyl ring, the AICAR imidazole ring, the NSC37173 benzyl ring, and the Phe316 benzyl ring form an aromatic "chain" involving both "edge-to-face" and "face-to-face"  $\pi$ - $\pi$  stackings, which may play a significant role in ligand binding and enzyme dynamics. (c) The amine group on the naphthalene ring hydrogen-bonds to the carbonyl backbone of Met313 and the side chain of Asn489.

Overall, in the case of docking NSC37173 to AICAR Tfase active site with AICAR substrate, the predicted binding mode of NSC37173 is very similar to that of BW1540 and BW2315, two potent sulfonyl-containing antifolates.<sup>38</sup>

**NSC292213.** This compound has a low  $IC_{50}$  of 8.8  $\mu$ M and molecular weight of 430 Da. Unlike NSC37173, it docks in the AICAR substrate binding site (Figure 2C). For half of the symmetric NSC292213, the carboxylate group interacts with the phosphate binding site through electrostatic and hydrogen-bonding interactions. The hydroxyl group H-bonds with Asn239 and the naphthalene occupies the AICAR ribose binding site and part of a side pocket (side chains of Ile238, Asn239, and Asp242 and main chains of Phe265, Lys266 and His267)

below the ribose binding site. For the other half, the carboxylate interacts with the "oxyanion hole" through electrostatics and H-bonds. The naphthalene ring interacts with Phe591 aromatically through "edge-to-face"  $\pi$  stacking. NSC292213 cannot be docked with AICAR in the active site, strongly suggesting that it binds mainly in the AICAR binding site and not the folate binding site.

**NSC326203.** This compound is a chemical dye with various commercial names, such as bucolan yellow or acid yellow 54. Docking to the AICAR Tfase active site with and without the chromium ion both show that the sulfate groups at both ends of the molecule have strong interactions with the "oxyanion hole" through primarily electrostatic interactions and also H-bonding in the different docking clusters. However, in this case, even though the simulated binding free energy is comparable to that of NSC37173 and NSC292213, docking cannot confidently predict its exact binding mode with AICAR Tfase because 12 clusters of predicted binding modes were obtained without any one showing clear preference over the others. This case may indicate the need to incorporate the aromatic interaction explicitly in the docking scoring functions and the need to develop polarizable force fields in molecular modeling and molecular dynamics in general.

**NSC88915.** The primary binding interactions of this compound come from its aromatic benzene stacking into the folate pterin pocket and its "electron-rich"  $-(O=)S-(=O)-O-$  linker interacting with the AICAR Tfase "oxyanion hole". Like most of the nonbinders indicated above, the simple "space-filling" of the steroidal rings shows little specific interaction with the active site, which may explain why the calculated binding affinity is so high, yet its  $IC_{50}$  is only modest.

**NSC26699.** This compound is an analogue of NSC3-7173 both in its topology and in its binding mode to the AICAR Tfase active site. The aminobenzene ring stacks into the folate pocket. The  $-C(=O)-NH-$  linker and sulfate interact with the proposed "oxyanion hole". Like NSC37173, its docking to AICAR Tfase with and without AICAR substrate result in high confidence for the predicted binding mode. The benzthiozole ring seems not to contribute much to the overall binding free energy.

The three compounds described below are weaker inhibitors with larger  $IC_{50}$  values compared to the previous five compounds but for different reasons.

**NSC321237.** This candidate is basically a 6-thioguanosine coordinated with benzylamine through a mercury ion. As a nucleoside analogue, its occupancy of the AICAR binding site is not surprising. Since no phosphate or sulfate is attached to the ribose 5'-OH, its binding is much weaker than the AICAR substrate (NSC321237  $IC_{50}$  is 105.9  $\mu$ M, whereas the  $K_m$  of AICAR is 16  $\mu$ M).

**NSC326211.** This compound is similar to NSC292213 except that its middle linker is much more rigid than the dicarbonyl linker of NSC292213 due to a benzene attached to the linker. The docking simulation also shows a similar binding mode for the two compounds. The extra benzene in the linker sits on the Asp339 side-chain carboxylate. This unfavorable benzene/carboxylate interaction would then weaken the binding of NSC32-6211 despite other favorable interactions compared to

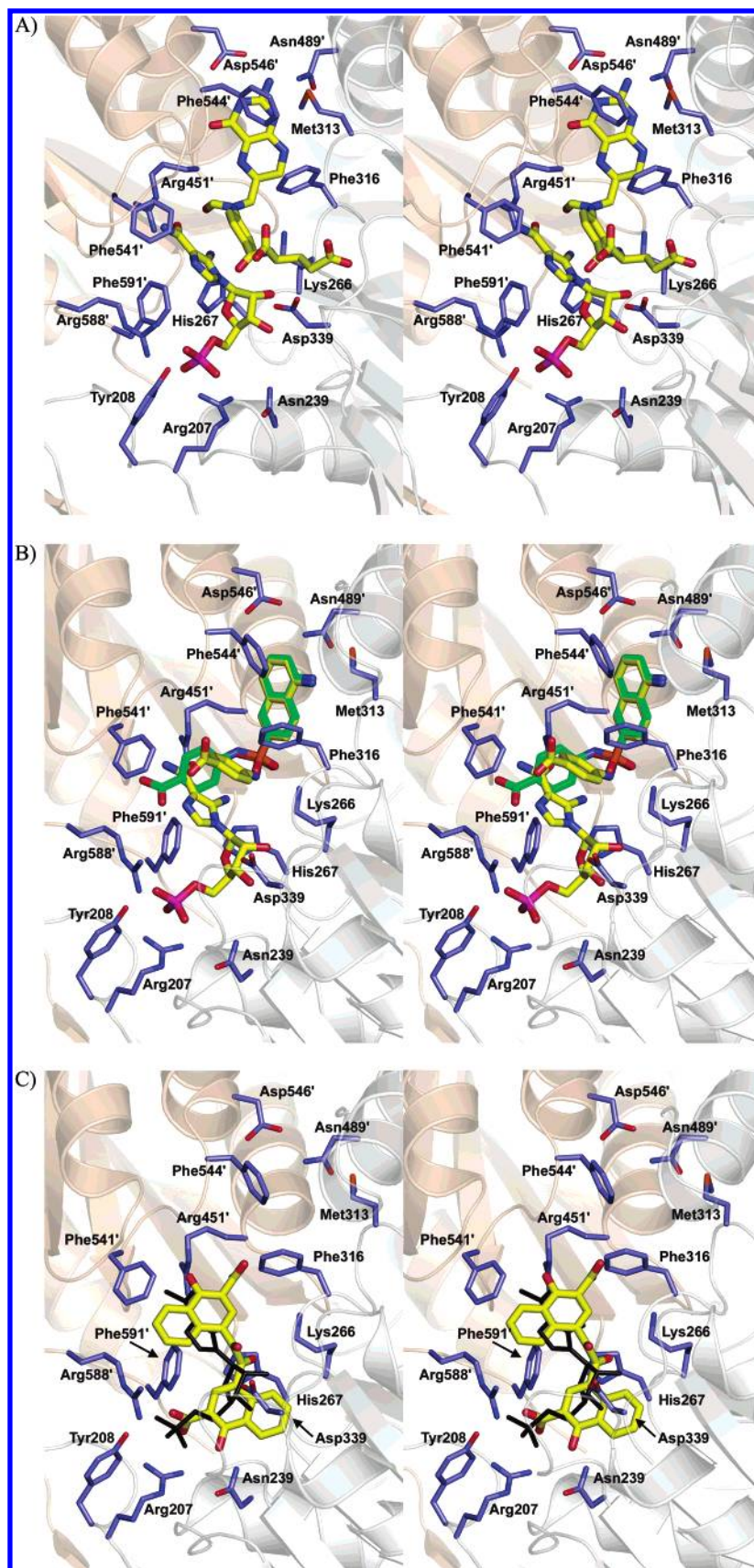


**Figure 2.** Folate cofactor and selected inhibitors binding to AICAR Tfase active site. (A) AICAR Tfase active site. The lower ligand is AICAR substrate identified by X-ray crystallography. The upper ligand is the folate cofactor docked via AutoDock. (B) NSC37173 binds to the active site. The lower ball-and-stick ligand is the crystallographic AICAR binding position. The upper ball-and-stick ligand is the docked position of NSC37173 with AICAR present. The green stick model is the docked position of NSC37173 without AICAR present (empty active site). (C) NSC292213 binds to the active site. The black stick model is the crystallographic AICAR binding position. The ball-and-stick ligand is the docked position of NSC292213 into an empty active site.



NSC292213.

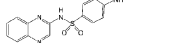
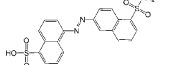
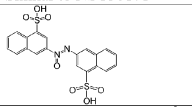
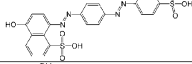
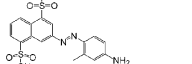
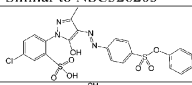
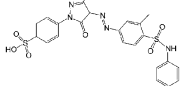
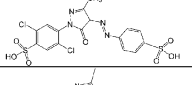
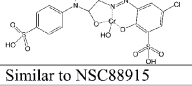
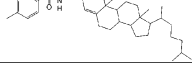
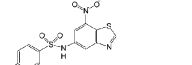
**NSC7524.** This is the weakest predicted inhibitor found from the diversity set yet with the highest molecular weight. Again the main interactions come from aromatic stacking in the folate binding pocket with Phe544 and the carboxylic linker interaction with the "oxyanion hole". The difference is that the carboxylic linker is less "electron-rich" than the sulfonamide and sulfoxyl linkers of NSC37173 and NSC88915, respectively. Thus, a much higher  $IC_{50}$  is not surprising. Like NSC88915 and the nonbinders, the simple "space-filling" of the fused ring moiety does not contribute to the overall binding ability.

**Inhibitors from the Complete NCI Database through Similarity Compound Searching.** Because the diversity set is a limited compound collection of unique pharmacophore profiles, related compounds are present in the complete NCI database with similar structural topologies and pharmacophore properties. The complete NCI database could contain compounds with comparable or stronger inhibition potentials than their diversity set analogues. Thus, a similar compound search and docking screen were carried out for the above inhibitors in the NCI database. All of the inhibitors that were found from the NCI structural database through similar compound searching and AutoDock screening, with the above five lower  $IC_{50}$  inhibitors as "seeds", are listed in Table 2.

**Inhibitors Related to NSC37173.** Seventy-seven compounds similar to NSC37173 were virtually screened through the same docking protocol as for the diversity set. Six compounds were selected for AICAR Tfase kinetic inhibition analysis on the basis of their docking free energies and conformational clustering. Four out of the six compounds precipitated in the assay solution. However, the remaining two compounds, NSC41806 and NSC30171, were both found to be AICAR Tfase inhibitors. NSC41806 is predicted to bind very similarly to NSC37173 as expected because of their close structural similarity. Compared to NSC37173, its binding is more than 10-fold weaker due to the lack of the amine H-bonding interactions in the folate pocket, and possibly weaker interactions between the "oxyanion hole" and the "switched" sulfonamide linker. On the other hand, NSC30171 was a surprise. Although this compound was picked out through NSC37173 similarity searching, its topology looks quite different from NSC37173. Enzymatic testing revealed that it is the most potent inhibitor found through our virtual screening thus far ( $K_i$  154 nM and  $IC_{50}$  600 nM). Docking with and without AICAR substrate in the active site indicates strongly that it competes with AICAR substrate for the AICAR binding site and hence is very different from NSC37173 and NSC41806. Key interactions with the AICAR Tfase active-site residues appear to be the electrostatic and H-bonding interactions between its sulfate and the enzyme "oxyanion hole", and the aromatic stacking of the naphthalene ring with the Phe590 benzyl ring. Thus, a NSC30171 similarity search was performed.

**Inhibitors Related to NSC30171.** Eight similar compounds were picked out for docking simulations, and three of them were subsequently tested for the AICAR Tfase kinetic inhibition. All three compounds were found

**Table 2.** AICAR Tfase Inhibitors from the Larger NCI-3D Database through Similarity Compound Searching and Docking Screening, and Enzymatic Inhibition Assays

Chemical structure	NSC number	MW	Rotatable bonds	% lowest energy clustering	$E_{\text{binding}}$ (Kcal/mol)	$IC_{50}$ ( $\mu$ M)
Similar to NSC37173						
	41806	342	5	66	-10.7	$54.7 \pm 11.5$
	30171	441	5	85	-11.7	$0.6 \pm 0.06$
Similar to NSC30171						
	37031	458	4	36	-12.4	$7.8 \pm 1.1$
	45592	559	7	41	-12.3	$11.6 \pm 0.4$
	58046	467	5	63	-12.0	$7.6 \pm 0.4$
Similar to NSC326203						
	47729	586	7	14	-12.8	$3.3 \pm 0.7$
	324572	551	7	15	-12.5	$11.6 \pm 0.9$
	324981	553	5	12	-12.2	$20.1 \pm 0.7$
	324571	600	6	10	-12.1	$20.1 \pm 0.7$
Similar to NSC88915						
	126445	553	8	20	-15.1	$9.6 \pm 0.8$
Similar to NSC26699						
	170645	349	4	72	-10.3	$36.1 \pm 1.7$

to be AICAR Tfase inhibitors with low  $IC_{50}$ , and all are predicted to bind similarly to NSC30171 (see Table 2).

**Inhibitors Related to NSC292213.** Ten similar compounds were selected for docking and two of them were selected for experimental testing on the basis of their docking free energies. Unfortunately, they have not been available for testing so far because NCI could not send the compounds.

**Inhibitors Related to NSC326203.** Ten similar compounds were docked and four were tested. Again all four are AICAR Tfase inhibitors (Table 2). These compounds are very similar structurally to NSC326203, and similar binding modes are expected. As for NSC-326203, docking shows large numbers of conformational clusters with similar binding free energies and without clear preferences for any particular cluster mode(s).

**Inhibitors Related to NSC88915.** Nineteen similar compounds were docked and six of them were selected for testing. Four of them precipitated in the solution, one is inactive, and one was found to be AICAR Tfase inhibitor (NSC126445 in Table 2). The compound has slightly lower  $IC_{50}$  than NSC88915. Docking shows that the aromatic ring is pushed further into the folate pocket, resulting in a stronger aromatic interaction with Phe544. The "electron-rich" linker is also slightly closer

to the AICAR Tfase "oxyanion hole".

**Inhibitors Related to NSC26699.** Fourteen similar compounds were docked and NSC170645 was suggested for enzymatic testing, which confirmed it as an inhibitor. Its binding to AICAR Tfase is slightly weaker with a similar binding mode to NSC26699. The loss of amine H-bonding to Asp546 may be the reason for weaker binding.

## Discussion

**Virtual Ligand Screening.** Virtual screening has been widely used to discover new lead compounds for drug design.<sup>52,53</sup> Successful studies have resulted with discovery of molecules either resembling the native ligands of the specific targets or novel leads.<sup>54–60</sup> This study is no exception, as compounds similar to the AICAR substrate (NSC321237), as well as novel scaffolds were identified. The initial *in vitro* inhibition assay on the NCI diversity set resulted in a very high success rate of 50% (eight inhibitors out of 16 soluble compounds). The secondary screening, coupled with structural similarity searching, increased the success rate to 92% (11 inhibitors out of 12 compounds). In all inhibitor classes, the docked conformations of the secondary screening hits matched the docked conformation of their lead inhibitor discovered in the first-round screening. This approach resembles the so-called hierarchical filtering. In our case, the first pass was used to discover the appropriate scaffolds through focusing on compound structural diversity. At this stage, utilization or construction of a structurally diverse library is the key. The second pass was to uncover the best analogues of the compounds discovered in the first pass. Examples of other kinds of hierarchical docking include multi-resolutional approaches of the Klebe group<sup>61</sup> and the Goddard group,<sup>62</sup> etc.

All of the eight inhibitors from the diversity set surprisingly inhibit at the micromolar level, with the highest IC<sub>50</sub> being 231.3  $\mu$ M and the lowest 4.1  $\mu$ M, corresponding to a binding free energy difference of about 2.4 kcal/mol. This is comparable to the 2.1 kcal/mol standard deviation of AutoDock scoring function, on which the selection of those 44 initial compounds was based. However, like all other docking programs, AutoDock cannot correctly rank all the inhibitors through a docking simulation if the binding free energy range is within the standard deviation, except if the compounds are structurally very similar. For example, NSC37173 and NSC41806 have the experimental  $\Delta\Delta G$  of  $RT \ln (IC_{50} \text{ of NSC37173} / IC_{50} \text{ of NSC41806}) = 1.36 \log (4.1/54.7) = -1.5$  kcal/mol, close to the predicted  $-12.5 - (-10.7) = -1.8$  kcal/mol. The correct ranking of the structurally related compounds NSC47729, NSC324572, NSC324981, and NSC324571 was also predicted. This result is notable because it is very useful in lead optimization during the drug design cycle once the main scaffolds are confirmed and ensuing combinatorial designs are initiated on those scaffolds.

**The Ranking Issue and the Scoring Functions.** Tremendous efforts have been made to improve the rank order of ligand compounds that are predicted to bind to a specific target over the years. The most rigorous ways to calculate relative binding free energy differences are free energy perturbation (FEP) and thermodynamic

integration (TI).<sup>63–65</sup> However, their expensive computational cost and required time render them impractical in the drug design screening stage at present. They are suitable for calculating the free energy differences among very similar compounds and are not viable for lead generation for a long time to come. As is well documented, docking programs inherently have sampling limitations, especially for the protein component (i.e., protein flexibility), and do not address the whole thermodynamic cycle. One way to solve these problems is to carry out a docking/screening on the large databases first and then proceed with detailed free energy analysis on the top binders.<sup>66</sup> For example, HierDock/HierVLS<sup>60,62</sup> has integrated the two calculations into one protocol. Another way is to carry out a completely different kind of postdocking processing not involving costly free energy evaluation. For example, binary kernel discrimination, support vector machine (SVM), trend vector analysis, and similarity searching/substructure analysis<sup>67</sup> are increasingly used once a training set is available. Another popular approach is to manipulate the scoring functions as summarized here: (a) Some studies show that a consensus scoring function combining three or four individual functions from different docking programs proves superior to a single one.<sup>68–71</sup> (b) A simple energy minimization following docking would improve the ranking,<sup>72</sup> especially after grid-based docking. (c) A molecular weight correction is applied to normalize the binding free energy contribution<sup>73</sup> since docking is usually biased toward the selection of high molecular weight compounds, which is exactly what happened in our case. For example, the simple high molecular weight "space-filling" of eight nonbinders in the diversity set gave high simulated binding free energies, yet in fact appear to contribute very little to binding to AICAR Tfase. However, one major advantage of AutoDock is the feasibility to train the scoring function coefficients of various energy terms to customize the function to a specific target like AICAR Tfase or to a specific class of targets, such as carbohydrate receptors.<sup>74</sup> Indeed, the AutoDock scoring function calibration to carbohydrate receptors downweights the van der Waals contribution to almost half the original (the coefficient for van der Waals term is reduced to 0.0737 from 0.1485) and upweights the electrostatic contribution almost 3-fold (from 0.1146 to 0.3330). AICAR Tfase has similar characteristics in that the binding forces mainly come from electrostatic, aromatic, and H-bonding, not van der Waals interactions.

**Characteristics of the AICAR Tfase Active Site and Its Inhibitors.** AICAR Tfase is a symmetrical homodimer with each monomer being composed of 393 residues. Both active sites are correspondingly located at the dimer interface with key active-site residues being contributed from both monomers. AICAR Tfase is unique among folate-binding enzymes for several reasons: (a) Its most striking features are its "oxyanion hole" consisting of Lys266, Arg451, and its backbone amide in the center of the active-site cleft, similar to the so-called "oxyanion hole" of  $\alpha/\beta$  hydrolases, and an additional helix dipole consisting of residues 450–468 with its N-terminus pointing toward the "oxyanion hole". Considering the weak nucleophilicity of the 5-amino group of AICAR and the overall reaction



direction favoring the reactants, this "oxyanion hole" is likely to be particularly important for the stabilization of the transition state during the formyl transfer. In addition, Lys266 may play a leading catalytic role. All of the inhibitors found in the virtual screening here have either an "electron-rich" linker  $[-(O=S(=O)-NH-]$ ,  $[-(O=S(=O)-O-]$ ,  $[-C(=O)-NH-]$ , or  $[-C(=O)-O-]$  or an "electron-rich" terminal group ( $-SO_3^-$ ) or both. This feature appears to be the most critical "hot spot" for future inhibitor design and is consistent with the conclusions drawn from the crystal structures of ATIC complexed with the sulfonyl-containing antifolates.<sup>38</sup>

(b) The second important feature of the AICAR Tfase active site is its aromatic system composed of residues Phe316, Phe591, Phe544, and Phe541, which play a critical role in anchoring and orienting the substrate AICAR and cofactor folate for binding and catalysis. As shown in the crystal structures and docking studies of folate cofactor and NSC37173, the aromatic stacking of Phe591, the imidazole of AICAR, the benzene of the folate, and Phe316 essentially "locate and orient" the enzyme-substrate-cofactor ternary complex for catalysis. This type of synergistic binding was also observed previously for thymidylate synthase complexed with a purine nucleotide and a folate mimic 1843U89.<sup>75</sup> Again, all of the inhibitors identified here contain at least one aromatic moiety that mostly binds into the pterin binding pocket and stacks with Phe544, or more frequently, have two aromatic moieties linked by a "electron-rich" linker. The second aromatic moiety normally interacts with Phe316 or Phe541 depending on the "perturbation" from the rest of the inhibitors. Effective utilization of an aromatic system seems the second design principle for AICAR Tfase inhibitors. The above two features play a defining role in developing useful pharmacophores and in selecting useful novel scaffolds.

(c) Unlike TS, DHFR, or GAR Tfase, AICAR Tfase does not undergo large conformational change upon ligand binding. The most noticeable changes are for Arg207 side chain, which moves in for phosphate/sulfate binding, the Phe544/Phe316 side-chain rotations for aromatic modulation, and a slight "closing-in" of the Pro543-Phe544-Arg545-Asp546 loop for a more constricted pterin pocket. From a drug designer's perspective, a more predictive behavior of the designed ligands and a more reliable free energy assessment should be expected with this type of "pre-formed" active site. However, sequestered structural waters may, in some cases, play an unexpected role that is difficult to predict.

**New Lead Generation through Linking of Sub-site Binders.** NSC37173 and NSC292213 bind to the AICAR Tfase cofactor and substrate binding sites, respectively. So it is possible that a covalent link between these two low  $IC_{50}$  inhibitors would create a new lead with increased potency and specificity. In principle, all of the above inhibitors, substrate/cofactor and their analogues, can be linked in various ways to generate possible "multisubstrate adduct" inhibitors. In fact, drug discovery through component assembly, such as fragment tethering, has been explored.<sup>76</sup>

**NCI Diversity Set.** The NCI diversity set covers a wide range of structural space<sup>77</sup> and the larger NCI-3D database contains a greater number of unique compounds, compared to other databases.<sup>78</sup> However, clear

limitations are apparent: (a) the diversity set is focused on the synthetic chemical space. Nature has a far richer diversity. A constantly updated "diversity set" that integrates natural products is needed; (b) a surprisingly large number of the NCI compounds are not soluble in the assay solution or precipitate with other chemicals in the buffer solution, as found for 28 out of 44 compounds in our enzymatic assay. It may not be as critical an issue in the cell-based assays for which the compounds have been curated at NCI. However, the solubility issue is important for molecular assays. Thus, a "cleaner" database is clearly preferred. The Shoichet group has found that many "promiscuous" compounds "inhibit" their targets nonspecifically and noncompetitively by forming large aggregates with a typical size of hundreds of nanometers in diameters<sup>79</sup> due to their inappropriate solubility profiles. These "false positives" are common in both public and corporate databases and should be removed, experimentally, by methods such as adding detergents,<sup>80</sup> and/or computationally before virtual screening, thus avoiding the time wasted chasing false "leads". The inhibitors of AICAR Tfase found here are not promiscuous inhibitors because their enzyme assays show typical competitive inhibition. Additionally, the nature of the inhibition did not change under 0.1 mg/mL saponin incubation. Finally, cell-based assays (data not shown) show that these inhibitors target more than just AICAR Tfase in the cell. Further improvements on their potency and especially specificity for AICAR Tfase, as well as considerations of their druglike properties, are currently underway.

**Acknowledgment.** We thank Garrett M. Morris, William "Lindy" Lindstrom, Ruth Huey, Michel Sanner, and David S. Goodsell for valuable suggestions and discussions. L.X. thanks the Susan G. Komen Fellowship for funding. This work was supported by the National Institutes of Health Grants P41 RR08605 (A.J.O. from NCBR), PO1 CA63536 (I.A.W.), and the National Cancer Institute Grant R24 CA95830 (A.J.O.).

## References

- (1) Jackman, A. L. *Antifolate drugs in cancer therapy*; Humana Press: Clifton, NJ, 1999.
- (2) Davies, J. F. D.; Delcamp, T. J.; Prendergast, N. J.; Ashford, V. A.; Freisheim, J. H.; Kraut, J. Crystal structures of recombinant human dihydrofolate reductase complexed with folate and 5-deazafoate. *Biochemistry* **1990**, *29*, 9467-9479.
- (3) Oefner, C.; D'Arcy, A.; Winkler, F. K. Crystal structure of human dihydrofolate reductase complexed with folate. *Eur. J. Biochem.* **1988**, *174*, 377-385.
- (4) Montfort, W. R.; Perry, K. M.; Fauman, E. B.; Finer-Moore, J. S.; Maley, G. F.; Hardy, L.; Maley, F.; Stroud, R. M. Structure, multiple site binding, and segmental accommodation in thymidylate synthase on binding dUMP and an anti-folate. *Biochemistry* **1990**, *29*, 6964-6977.
- (5) Hardy, L. W.; Finer-Moore, J. S.; Montfort, W. R.; Jones, M. O.; Santi, D. V.; Stroud, R. M. Atomic structure of thymidylate synthase: Target for rational drug design. *Science* **1987**, *235*, 448-455.
- (6) Newell, D. R. Clinical pharmacokinetics of antitumor antifolates. *Semin. Oncol.* **1999**, *26*, 74-81.
- (7) Takimoto, C. H. Antifolates in clinical development. *Semin. Oncol.* **1997**, *24*, S18-40-S18-51.
- (8) Christopherson, R. I.; Lyons, S. D.; Wilson, P. K. Inhibitors of *de novo* nucleotide biosynthesis as drugs. *Acc. Chem. Res.* **2002**, *35*, 961-971.
- (9) Boger, D. L.; Marsilje, T. H.; Castro, R. A.; Hedrick, M. P.; Jin, Q.; Baker, S. J.; Shim, J. H.; Benkovic, S. J. Design, synthesis, and biological evaluation of fluoronitrophenyl substituted folate analogues as potential inhibitors of GAR transformylase and AICAR transformylase. *Bioorg. Med. Chem. Lett.* **2000**, *10*, 1471-1475.

- (10) Zhang, Y.; Desharnais, J.; Marsilje, T. H.; Li, C.; Hedrick, M. P.; Gooljarsingh, L. T.; Tavassoli, A.; Benkovic, S. J.; Olson, A. J.; Boger, D. L.; Wilson, I. A. Rational design, synthesis, evaluation, and crystal structure of a potent inhibitor of human GAR Tfase: 10-(Trifluoroacetyl)-5,10-dideazaacyclic-5,6,7,8-tetrahydrofolic acid. *Biochemistry* **2003**, *42*, 6043–6056.
- (11) Mueller, W. T.; Benkovic, S. J. On the purification and mechanism of action of 5-aminoimidazole-4-carboxamide-ribonucleotide transformylase from chicken liver. *Biochemistry* **1981**, *20*, 337–344.
- (12) Jackson, R. C.; Harkrader, R. J. In *Nucleosides and Cancer Treatment*; Tattersall, M. H. N., Fox, R. M., Eds.; Academic Press: Sydney, Australia, 1981; pp 18–31.
- (13) Christopherson, R. I.; Duggleby, R. G. Metabolic resistance: the protection of enzymes against drugs which are tight-binding inhibitors by the accumulation of substrate. *Eur. J. Biochem.* **1983**, *134*, 331–335.
- (14) Bebenek, K.; Roberts, J. D.; Kunkel, T. A. The effects of dNTP pool imbalances on frameshift fidelity during DNA replication. *J. Biol. Chem.* **1992**, *267*, 3589–3596.
- (15) Meyn, R. E.; Stephens, L. C.; Hunter, N. R.; Milas, L. Apoptosis in murine tumors treated with chemotherapy agents. *Anticancer Drugs* **1995**, *6*, 443–450.
- (16) Nord, L. D.; Stolfi, R. L.; Alfieri, A. A.; Netto, G.; Reuter, V.; Sternberg, S. S.; Colofiore, J. R.; Koutcher, J. A.; Martin, D. S. Apoptosis induced in advanced CD8F1-murine mammary tumors by the combination of PALA, MMPR and 6AN precedes tumor regression and is preceded by ATP depletion. *Cancer Chemother. Pharmacol.* **1997**, *40*, 376–384.
- (17) Martin D. S.; Spriggs D.; Koutcher J. A. A concomitant ATP-depleting strategy markedly enhances anticancer agent activity. *Apoptosis* **2001**, *6*, 125–131.
- (18) Taylor, E. C.; Harrington, P. J.; Fletcher, S. R.; Beardsley, G. P.; Moran, R. G. Synthesis of the antileukemic agents 5,10-dideazaaminopterin and 5,10-dideaza-5,6,7,8-tetrahydroaminopterin. *J. Med. Chem.* **1985**, *28*, 914–921.
- (19) Beardsley, G. P.; Moroson, B. A.; Taylor, E. C.; Moran, R. G. A new folate antimetabolite, 5,10-dideaza-5,6,7,8-tetrahydrofolate is a potent inhibitor of de novo purine synthesis. *J. Biol. Chem.* **1989**, *264*, 328–333.
- (20) Baldwin, S. W.; Tse, A.; Gossett, L. S.; Taylor, E. C.; Rosowsky, A.; Shih, C.; Moran, R. G. Structural features of 5,10-dideaza-5,6,7,8-tetrahydrofolate that determine inhibition of mammalian glycylamide ribonucleotide formyltransferase. *Biochemistry* **1991**, *30*, 1997–2006.
- (21) Kamen, B. Folate and antifolate pharmacology. *Semin. Oncol.* **1997**, *24* (Suppl.), 18, 30–39.
- (22) Cronstein, B. N.; Naime, D.; Ostad, E. The antiinflammatory mechanism of methotrexate: Increased adenosine release at inflamed sites diminishes leukocyte accumulation in an in vivo model of inflammation. *J. Clin. Invest.* **1993**, *92*, 2675–2682.
- (23) Baggott, J. E.; Morgan, S. L.; Ha, T.; Vaughn, W. H.; Hine, R. J. Inhibition of folate-dependent enzymes by nonsteroidal antiinflammatory drugs. *Biochem. J.* **1992**, *282*, 197–202.
- (24) Allegra, C. J.; Drake, J. C.; Jolivet, J.; Chabner, B. A. Inhibition of phosphoribosylaminoimidazolecarboxamide transformylase by methotrexate and dihydrofolic acid polyglutamates. *Proc. Natl. Acad. Sci. U.S.A.* **1985**, *82*, 4881–4885.
- (25) Gadangi, P.; Longaker, M.; Naime, D.; Levin, R. I.; Recht, P. A.; Montesinos, M. C.; Buckley, M. T.; Carlin, G.; Cronstein, B. N. The antiinflammatory mechanism of sulfasalazine is related to adenosine release at inflamed sites. *J. Immunol.* **1996**, *156*, 1937–1941.
- (26) Chan, A. Y.; Soltys, C. L.; Young, M. E.; Proud, C. G.; Dyck, J. R. Activation of AMP-activated protein kinase inhibits protein synthesis associated with hypertrophy in the cardiac myocyte. *J. Biol. Chem.* **2004**, May 24. Epub ahead of print.
- (27) Lihn, A. S.; Jessen, N.; Pedersen, S. B.; Lund, S.; Richelsen, B. AICAR stimulates adiponectin and inhibits cytokines in adipose tissue. *Biochem. Biophys. Res. Commun.* **2004**, *316*, 853–8.
- (28) Giri, S.; Nath, N.; Smith, B.; Viollet, B.; Singh, A. K.; Singh, I. 5-aminoimidazole-4-carboxamide-1- $\beta$ -D-ribofuranoside inhibits proinflammatory response in glial cells: A possible role of AMP-activated protein kinase. *J. Neurosci.* **2004**, *24*, 479–487.
- (29) Hanauske, A. R.; Chen, V.; Paoletti, P.; Niyikiza, C. Pemetrexed disodium: A novel antifolate clinically active against multiple solid tumors. *Oncologist* **2001**, *6*, 363–373.
- (30) Erba, E.; Sen, S.; Sessa, C.; Vikhanskaya, F. L.; D'Incalci, M. Mechanism of cytotoxicity of 5,10-dideazatetrahydrofolic acid in human ovarian carcinoma cells in vitro and modulation of the drug activity by folic or folinic acid. *Br. J. Cancer* **1994**, *69*, 205–211.
- (31) Mendelsohn, L. G.; Shih, C.; Chen, V. J.; Habeck, L. L.; Gates, S. B.; Shackelford, K. A. Enzyme inhibition, polyglutamation, and the effect of LY231514 (MTA) on purine biosynthesis. *Semin. Oncol.* **1999**, *26*, 42–47.
- (32) Calvert, H. An overview of folate metabolism: features relevant to the action and toxicities of antifolate anticancer agents. *Semin. Oncol.* **1999**, *26*, 3–10.
- (33) Nair, M. G. Book review on “Antifolate Drugs in Cancer Therapy”. *Drug Discovery Today* **1999**, *4*, 492–494.
- (34) Cao, S.; Abraham, A.; Nair, M. G.; Pati, R.; Galivan, J. H.; Hausheer, F. H.; Rustum, Y. M. Polyglutamylation of the dihydrofolate reductase inhibitor gamma-methylene-10-deazaaminopterin is not essential for antitumor activity. *Clin. Cancer Res.* **1996**, *2*, 707–712.
- (35) Greasley, S. E.; Horton, P.; Ramcharan, J.; Beardsley, G. P.; Benkovic, S. J.; Wilson, I. A. Crystal structure of a bifunctional transformylase and cyclohydrolase enzyme in purine biosynthesis. *Nat. Struct. Biol.* **2001**, *8* (5), 402–406.
- (36) Wolan, D. W.; Greasley, S. E.; Beardsley, G. P.; Wilson, I. A. Structural insights into the avian AICAR transformylase mechanism. *Biochemistry* **2002**, *41*, 15505–15513.
- (37) Wolan, D. W.; Greasley, S. E.; Wall, M. J.; Benkovic, S. J.; Wilson, I. A. Structure of avian AICAR transformylase with a multisubstrate adduct inhibitor  $\beta$ -DADF identifies the folate binding site. *Biochemistry* **2003**, *42*, 10904–10914.
- (38) Cheong, C. G.; Wolan, D. W.; Greasley, S. E.; Horton, P. A.; Beardsley, G. P.; Wilson, I. A. Crystal structures of human bifunctional enzyme aminoimidazole-4-carboxamide ribonucleotide transformylase/IMP cyclohydrolase in complex with potent sulfonyl-containing antifolates. *J. Biol. Chem.* **2004**, *279*, 18034–18045.
- (39) [http://dtp.nci.nih.gov/branches/dscb/diversity\\_explanation.html](http://dtp.nci.nih.gov/branches/dscb/diversity_explanation.html).
- (40) Goodsell, D. S.; Olson, A. J. Automated docking of substrates to proteins by simulated annealing. *Proteins: Struct., Funct., Genet.* **1990**, *8*, 195–202.
- (41) Morris, G. M.; Goodsell, D. S.; Huey, R.; Olson, A. J. Distributed automated docking of flexible ligands to proteins: Parallel applications of AutoDock 2.4. *J. Comput.-Aided Mol. Des.* **1996**, *10*, 293–304.
- (42) Morris, G. M.; Goodsell, D. S.; Halliday, R. S.; Huey, R.; Hart, W. E.; Belew, R. K.; Olson, A. J. Automated docking using a Lamarckian genetic algorithm and empirical binding free energy function. *J. Comput. Chem.* **1998**, *19*, 1639–1662.
- (43) Weiner, S. J.; Kollman, P. A.; Case, D. A.; Singh, U. C.; Ghio, C.; Alagona, G.; Profeta, S.; Weiner, P. A new force field for molecular mechanical simulation of nucleic acids and proteins. *J. Am. Chem. Soc.* **1984**, *106*, 765–784.
- (44) Gasteiger, J.; Marsili, M. Iterative partial equalization of orbital electronegativity—a rapid access to atomic charges. *Tetrahedron* **1980**, *36*, 3219–3228.
- (45) Rowe, P. B. The synthesis of  $N^5,N^{10}$ -methenyltetrahydrofolic acid. In *Methods in Enzymology*; McCormick, D. B., Wright, L. D., Eds.; Academic Press: New York, 1971; Volume XVIII, pp 733–735.
- (46) Black, S. L.; Black, M. J.; Mangum, J. H. A rapid assay for 5-amino-4-imidazolecarboxamide ribotide transformylase. *Anal. Biochem.* **1978**, *90*, 397–401.
- (47) Boger, D. L.; Haynes, N.-E.; Warren, G. L.; Ramcharan, J.; Kito, P. A.; Benkovic, S. J. Functionalized analogues of 5,8,10-Trideazafofate: development of an enzyme-assembled tight binding inhibitor of GAR Tfase and a potential irreversible inhibitor of AICAR Tfase. *Bioorg. Med. Chem.* **1997**, *5*, 1839–1846.
- (48) Boger, D. L.; Haynes, N.-E.; Warren, M. S.; Gooljarsingh, L. T.; Ramcharan, J.; Kito, P. A.; Benkovic, S. J. Functionalized analogues of 5,8,10-Trideazafofates as potential inhibitors of GAR Tfase or AICAR Tfase. *Bioorg. Med. Chem.* **1997**, *5*, 1831–1838.
- (49) Xu, L.; Li, C.; Olson, A. J.; Wilson, I. A. Crystal structure of avian AICAR transformylase in complex with a novel inhibitor identified by virtual ligand screening. *J. Biol. Chem.*, in press.
- (50) Milne, G. W. A.; Nicklaus, M. C.; Driscoll, J. S.; Wang, S.; Zaharevitz, D. W. The NCI drug information system 3D database. *J. Chem. Inf. Comput. Sci.* **1994**, *34*, 1219–1224.
- (51) Chang, T. K.; Chiang, Y.; Guo, H.-X.; Kresge, A. J.; Mathew, L.; Powell, M. F.; Wells, J. A. Solvent isotope effects in  $H_2O$ – $D_2O$  mixtures (Proton Inventories) on serine-protease-catalyzed hydrolysis reactions: Influence of oxyanion hole interactions and medium effects. *J. Am. Chem. Soc.* **1996**, *118*, 8802–8807.
- (52) Kuntz, I. D. Structure-based strategies for drug design and discovery. *Science* **1992**, *257*, 1078–1082.
- (53) Walters, W. P.; Stahl, M. T.; Murcko, M. A. Virtual screening – An Overview. *Drug Discovery Today* **1998**, *3*, 160–178.
- (54) DesJarlais, R. L.; Seibel, G. L.; Kuntz, I. D.; Furth, P. S.; Alvarez, J. C.; Ortiz de Montellano, P. R.; DeCamp, D. L.; Babe, L. D.; Craik, C. S. Structure-based design of nonpeptide based inhibitors specific for the human immunodeficiency virus 1 protease. *Proc. Natl. Acad. Sci. U.S.A.* **1990**, *87*, 6644–6648.
- (55) Shoichet, B. K.; Stroud, R. M.; Santi, D. V.; Kuntz, I. D.; Perry, K. M. Structure-based discovery of inhibitors of thymidylate synthase. *Science* **1993**, *259*, 1445–1450.

- (56) Schevitz, R. W.; Bach, N. J.; Carlson, D. G.; Chirgadze, N. Y.; Clawson, D. K.; Dillard, R. D.; Draheim, S. E.; Hartley, L. W.; Jones, N. D.; Mihelich, E. D.; Olkowski, J. L.; Snyder, D. W.; Sommers, C.; Wery, J.-P. Structure-based design of the first potent and selective inhibitor of human nonpancreatic secretory phospholipase A2. *Nat. Struct. Biol.* **1995**, *2*, 458–465.
- (57) Emanuele, P.; Xu, K.; Kollmeyer, T. M.; Kaufmann, S. H.; Prendergast, F. G.; Pang, Y.-P. Successful virtual screening of a chemical database for farnesyltransferase inhibitor leads. *J. Med. Chem.* **2000**, *43*, 401–408.
- (58) Dunten, P.; Kammloft, U.; Crowther, R.; Levin, W.; Foley, L. H.; Wang, P.; Palermo, R. X-ray structure of a novel matrix metalloproteinase inhibitor complexed to stromelysin. *Protein Sci.* **2001**, *10*, 923–926.
- (59) Schapira, M.; Abagyan, R.; Totrov, M. Nuclear hormone receptor targeted virtual screening. *J. Med. Chem.* **2003**, *46*, 3045–3059.
- (60) Wely, B. F.; Vaidehi, N.; Zamanakos, G.; Goddard, W. A., III. HierVLS hierarchical docking protocol for virtual ligand screening of large-molecule database. *J. Med. Chem.* **2004**, *47*, 56–71.
- (61) Gruneberg, S.; Stubbs, M. T.; Klebe, G. Successful virtual screening for novel inhibitors of human carbonic anhydrase: strategy and experimental confirmation. *J. Med. Chem.* **2002**, *45*, 3588–3602.
- (62) Wang, P.; Vaidehi, N.; Tirrell, D. A.; Goddard, W. A., III. Virtual screening for binding of phenylalanine analogues to phenylalanyl-tRNA synthetase. *J. Am. Chem. Soc.* **2002**, *124*, 14442–14449.
- (63) Beveridge, D. L.; DiCapua, F. M. Free energy via molecular simulation: Applications to chemical and biomolecular systems. *Annu. Rev. Biophys. Biophys. Chem.* **1989**, *18*, 431–492.
- (64) Straatsma, T.; McCammon, A. Computational alchemy. *Annu. Rev. Phys. Chem.* **1992**, *43*, 407–435.
- (65) Kollman, P. A. Free energy calculations: Applications to chemical and biochemical phenomena. *Chem. Rev.* **1993**, *93*, 2395–2417.
- (66) Reddy, M. R.; Erion, M. D., Eds. *Free energy calculations in rational drug design*; Kluwer Academic/Plenum Publishers: New York, 2001.
- (67) Wilton, D.; Willett, P. Comparison of ranking methods for virtual screening in lead-discovery programs. *J. Chem. Inf. Comput. Sci.* **2002**, *43*, 469–474.
- (68) Wang, R.; Wang, S. How does consensus scoring work for virtual library screening? An idealized computer experiment. *J. Chem. Inf. Comput. Sci.* **2001**, *41*, 1422–1426.
- (69) Bissantz, C.; Folkers, G.; Rognan, D. Protein-based virtual screening of chemical databases. 1. Evaluation of different docking/scoring combinations. *J. Med. Chem.* **2000**, *43*, 4759–4767.
- (70) Stahl, M.; Rarey, M. Detailed analysis of scoring functions for virtual screening. *J. Med. Chem.* **2001**, *44*, 1035–1044.
- (71) Wang, R.; Lu, Y.; Wang, S. Comparative evaluation of 11 scoring functions for molecular docking. *J. Med. Chem.* **2003**, *46*, 2287–2303.
- (72) Wu, G.; Robertson, D. H.; Brooks, C. L., III; Vieth, M. Detailed analysis of grid-based molecular docking: A case study of CDOCKER – A CHARMM-based MD docking algorithm. *J. Comput. Chem.* **2003**, *24*, 1549–1562.
- (73) Pan, Y.; Huang, H.; Cho, S.; MacKerell, A. D., Jr. Consideration of molecular weight during compound selection in virtual target-based database screening. *J. Chem. Inf. Comput. Sci.* **2003**, *43*, 267–272.
- (74) Laederach, A.; Reilly, P. J. Specific empirical free energy function for automated docking of carbohydrates to proteins. *J. Comput. Chem.* **2003**, *24*, 1748–1757.
- (75) Weichsel, A.; Montfort, W. R.; Ciesla, J.; Maley, F. Promotion of purine nucleotide binding to thymidylate synthase by a potent folate analogue inhibitor 1843U89. *Proc. Natl. Acad. Sci. U.S.A.* **1995**, *92*, 3493–3497.
- (76) Erlanson, D.; Wells, J.; Braisted, A. Tethering: Fragment-based drug discovery. *Annu. Rev. Biophys. Biomol. Struct.* **2004**, *33*, 199–223.
- (77) Shi, L. M.; Fan, Y.; Lee, J. K.; Waltham, M.; Andrews, D. T.; Scherf, U.; Paull, K. D.; Weinstein, J. N. Mining and visualizing large anticancer drug discovery databases. *J. Chem. Inf. Comput. Sci.* **2000**, *40*, 367–379.
- (78) Voigt, J. H.; Bienfait, B.; Wang, S.; Nicklaus, M. C. Comparison of the NCI open database with seven large chemical structural databases. *J. Chem. Inf. Comput. Sci.* **2001**, *41*, 702–712.
- (79) McGovern, S.; Caselli, E.; Grigorieff, N.; Shoichet, B. K. A common mechanism underlying promiscuous inhibitors from virtual and high-throughput screening. *J. Med. Chem.* **2002**, *45*, 1712–1722.
- (80) Ryan, A. J.; Gray, N. M.; Lowe, P. N.; Chung, C.-W. Effect of detergent on “promiscuous” inhibitors. *J. Med. Chem.* **2003**, *46*, 3448–3451.

JM0495040